Biotinylated polyaminoacid-based nanoparticles for the targeted delivery of lenvatinib towards hepatocarcinoma

Paola Varvarà [a,b,1], Salvatore Emanuele Drago [a,1], Emanuela Esposito [c], Michela Campolo [c], Nicolò Mauro [a], Giovanna Calabrese [c], Sabrina Conoci [c,d,e], Dario Morganti [e], Barbara Fazio [e], Gaetano Giammona [a], Giovanna Pitarresi [a,*]

[a] Dipartimento di Scienze e Tecnologie Biologiche Chimiche e Farmaceutiche (STEBICEF), Università degli Studi di Palermo, Via Archirafi 32, Palermo 90123, Italy
[b] Fondazione Veronesi, Piazza Velasca 5, 20122 Milano, Italy
[c] Dipartimento Di Scienze Chimiche, Biologiche, farmaceutiche ed Ambientali (CHIBIOFARAM), via F. Stagno d'Alcontres 31, università degli Studi di Messina, Messina 98165, Italy
[d] Dipartimento di Chimica "Giacomo Ciamician", Alma Mater Studiorum, Università di Bologna, Italy
[e] LAB Sense Beyond Nano—URT Department of Sciences Physics and Technologies of Matter (DSFTM) CNR, Messina 98166, Italy

ARTICLE INFO

ABSTRACT

In this work, we describe the development of targeted polymeric nanoparticles loaded with lenvatinib for the treatment of hepatocellular carcinoma (HCC). A synthetic brush copolymer (PHEA-g-BIB-pButMA-g-PEG-biotin) was synthesized from α-poly(N-2-hydroxyethyl)-D,L-aspartamide (PHEA) by a three-step reaction involving atom transfer radical polymerisation (ATRP) to graft hydrophobic polybutylmethacrylate pendant groups and further conjugation with biotinylated polyethylene glycol via carbonate ester. Subsequently, lenvatinib-loaded nanoparticles were obtained and characterized demonstrating colloidal size, negative zeta potential, biotin exposure on the surface and the ability to release lenvatinib in a sustained manner. Lenvatinib-loaded nanoparticles were tested in vitro on HCC cells to evaluate their anticancer efficacy compared to free drug. Furthermore, the enhanced in vivo efficacy of lenvatinib-loaded nanoparticles on nude mice HCC xenograft models was demonstrated by evaluating tumor burdens, apoptotic markers and histological scores after administration of lenvatinib-nanoparticles via intraperitoneal or oral route. Finally, in vivo biodistribution studies were performed, demonstrating the ability of the prepared drug delivery systems to significantly accumulate in the solid tumor by active targeting, due to the presence of biotin on the nanoparticle surface.

1. Introduction

Hepatocellular carcinoma (HCC) is a primary liver cancer that arises from hepatocytes, the main functional cells of the liver (Bruix et al., 2019; Hu et al., 2023; Llovet et al., 2022; Llovet et al., 2021). It represents a substantial global health concern due to its high incidence and mortality rates (Jemal et al., 2011). Innovative therapeutic approaches are imperative to address the challenges posed by HCC and to enhance the overall efficacy of treatment strategies. Traditional treatment modalities, such as surgery, chemotherapy, and radiation therapy, have limitations in effectively managing HCC (Daher et al., 2018; Finn, 2013; Jemal et al., 2011). Surgery may not be feasible in advanced stages, and systemic chemotherapy often faces obstacles related to drug distribution, off-target effects, and drug resistance. Moreover, the liver's complex anatomy and functions make it a challenging organ for conventional therapeutic interventions (Anwanwan et al., 2020; Hu et al., 2023). In this landscape, the development of advanced drug delivery systems emerges as a promising avenue for improving the outcomes of HCC treatment (Fu et al., 2017; Hu et al., 2023; Liu et al., 2015; Wang et al., 2022; Yu et al., 2024). Advanced drug delivery systems are designed to overcome the limitations of traditional approaches by providing targeted and controlled release of therapeutic agents. These systems aim to enhance the therapeutic index of drugs, minimize side effects, and improve the overall efficacy of anticancer treatments (Böttger et al., 2020; Metkar et al., 2023; Scarabel et al., 2017). Targeted drug delivery allows for the specific delivery of therapeutic agents to the

---

tumor site while sparing healthy tissues (Böttger et al., 2020). This is crucial in HCC, where the precision of treatment is paramount for optimizing therapeutic benefits and minimizing collateral damage to the surrounding liver parenchyma. Moreover, the development of drug delivery systems offers the opportunity to address challenges related to the physicochemical properties of anticancer drugs (e.g., poor solubility, instability) such as multiple kinase inhibitors like lenvatinib (Anwanwan et al., 2020; Capozzi et al., 2019; Luo et al., 2023). This latter has been approved by the American Food and Drug Administration for several cancers, including HCC, thyroid cancer, and metastatic renal cell carcinoma (Wang et al., 2024). It acts on multiple molecular targets such as VEGFR1–3, FGFR1–4, PDGFR, KIT (stem cell factor receptor), and RET (rearranged during transfection), which are known drivers in cancer. This mechanism enables lenvatinib to exhibit antitumor and immunomodulatory effects in various preclinical cancer models, particularly in HCC (Zhao et al., 2020). Its mode of action allows it to influence tumor growth also due to its antiangiogenic activity, leading to tumor ischemia and hypoxia in the tumor microenvironment, thereby suppressing tumor growth and inducing tumor cell death. Efficient delivery of lenvatinib is crucial for optimizing its therapeutic efficacy, addressing the need for targeted drug delivery systems to enhance its specific action at the HCC site and minimize potential side effects. Nanomedicine, a subset of drug delivery systems utilizing nanotechnology, has gained considerable attention in the field of cancer therapy, including HCC (Landesman-Milo and Peer, 2016; Mauro et al., 2022). Nanoparticles, liposomes, micelles, and other nano-sized carriers can be engineered to encapsulate lenvatinib and navigate the intricate biological barriers to reach cancer cells selectively (Al-Salama et al., 2019; Böttger et al., 2020; Giammona et al., 2022a; Landesman-Milo and Peer, 2016). Additionally, the surface modification of these nanocarriers with targeting ligands allows for site-specific drug delivery, further enhancing treatment precision (Giammona et al., 2022a; Hu et al., 2015; Landesman-Milo and Peer, 2016; Singh et al., 2023). These innovative systems offer the potential to overcome challenges associated with conventional therapies, providing targeted and efficient delivery of therapeutic agents to improve outcomes for patients with HCC. In this context, this study focuses on the design and synthesis of biotin-conjugated polymeric nanoparticles for the targeted delivery of the emerging drug, lenvatinib, known for its efficacy in HCC treatment. The initial step involved the controlled polymerization of a polymeric derivative via Atom Transfer Radical Polymerization (ATRP), chosen for its capability to tailor polymers with well-defined structures crucial for biomedical applications. Previous studies have highlighted the success of synthesizing amphiphilic brush copolymers, specifically poly(2-hydroxyethyl-D,L-aspartamide) (PHEA) as the hydrophilic backbone and hydrophobic polybutylmethacrylate pendant groups, demonstrating noteworthy efficacy in hepatocarcinoma drug delivery. The potential of this copolymer was further augmented by integrating biotin as a targeting agent, due to overexpression of biotin receptor in HEPG2 cells (Chen et al., 2019), enhancing the selectivity of hepatocarcinoma treatment. To evaluate the therapeutic efficacy, in vitro and in vivo studies were conducted, encompassing both oral and intraperitoneal administrations of lenvatinib loaded nanoparticles. The purpose of this work is to report on the capabilities of the developed nanosystem.

2. Materials and methods

2.1. Materials

2-bromoisobutyryl bromide (BIBB), butyl methacrylate (ButMA), dimethylacetamide (DMA), dimethylformamide (DMF), methanol (MeOH), copper bromide (Cu^{I}Br), 2,2′-bipyridyl (Bpy), triethylamine (TEA), Bis (4-nitrophenyl) carbonate (BNPC), polyvinylpyrrolidone 40 KDa (PVP), diethyl ether, HABA/Avidin Reagent, Dulbecco's phosphate buffer saline (DPBS), NaOH, HCl and biotin-dPEG®$_{11}$-NH$_2$ (PEG chain ≈ 500 Da) were purchased from Merck (Italy). Lenvatinib mesylate was

purchased from D.B.A. Italia s.r.L. (Italy). All materials used for biological characterization were were purchased from Merck (Italy). The monomethyl ether hydroquinone present in the commercially available ButMA (used as stabilizing agent) was removed through basic activated aluminium oxide column. α, β-poly(N-2-hydroxyethyl)-D,L-aspartamide (PHEA) was synthesized by complete aminolysis of polysuccinimide (PSI) using ethanolamine in a DMF solution and purified following a previously reported procedure (Giammona et al., 1987). The spectroscopic data confirm the structure of the polymer. ^{1}H NMR (300 MHz, D$_2$O, 25 °C, TMS): δ 2.71 (m, 2H PHEA, –COCHCH$_2$CONH–), δ 3.24 (m, 2H PHEA, –NHCH$_2$CH$_2$O–), δ 3.55 (m, 2H PHEA, –NHCH$_2$CH$_2$OH), δ 4.59 [m, 1H PHEA, –NHCH(CO)CH$_2$–].

2.2. General procedure for the derivatization of PHEA with 2-bromoisobutyryl bromide

The synthesis of the PHEA-g-BIB copolymer followed a previously published procedure (Cervello et al., 2017). In brief, 500 mg of PHEA (3.1 mmol of OH) was dissolved in 10 mL of anhydrous DMA at room temperature. Subsequently, 440 µL of TEA were added, setting a molar ratio of 1 between TEA and PHEA hydroxyl groups. The reaction mixture was then cooled to 0 °C, and 390 µL of BIBB (molar ratio of 1 between BIBB/PHEA hydroxyl groups) were added to the flask under vigorous stirring. After maintaining the reaction at room temperature for 4 h, the flask content was dripped into cold diethyl ether. The resulting precipitate underwent two washes with the same solvent, and the residue was desiccated at low pressure, further purified by dialysis (MWCO 12–14 kDa), and finally, freeze-dried.

^{1}H NMR (300 MHz, DMF-d7, 25 °C) δ: 1.95 (s, 6H BIB, (CH$_3$)$_2$-C-CO-), 3.29 (m, 2H PHEA, –NHCH$_2$CH2O–), 3.58 (m, 2H PHEA, –NHCH$_2$CH$_2$OH), 4.25 (m, 2H PHEA, –NHCH$_2$CH$_2$O-BIB), 4.76 (m, 1H PHEA –NHCH(CO)CH$_2$–).

2.3. General procedure for the derivatization of PHEA-BIB with poly (butyl methacrylate) through ATRP

The PHEA-g-BIB-pButMA copolymer was synthesized according to a procedure already reported (Cervello et al., 2017). In detail, 150 mg of PHEA-g-BIB (equivalent to 0.255 mmol of BIB) were dissolved in 12 mL of a pre-degassed mixture of 1:1 anhydrous DMF/MeOH (v/v). To this solution, 400 µL of butylmethacrylate were added, maintaining a molar ratio of 10 between the ButMA monomer and BIB. Afterward, under vigorous stirring and argon bubbling, 35.8 mg of Cu^{I}Br catalyst (mol Cu^{I}Br/mol BIB in the polymer side chain equal to 1) and 156.18 mg of bipyridine (Bpy) (mol Bpy/mol Cu^{I}Br equal to 4) were mixed with a spatula and then introduced into the mixture. The reaction proceeded under an argon atmosphere at 50 °C for 20 h, and upon completion, the flask was opened to stop the process. The resulting polymer was isolated by slowly dripping the reaction mixture into a 1:1 water/MeOH mixture, and the precipitate was washed twice with the same mixture. The obtained white residue was dissolved in DMF, purified by dialysis (MWCO 12–14 kDa), and finally freeze-dried.

^{1}H NMR (300 MHz, DMF-d7, 25 °C, TMS) δ: 0.99 (m, 6H ButMA, –CH-CH$_3$ and –CH$_2$-CH$_2$-CH$_3$), 1.48 (m, 2H ButMA, –CH$_2$-CH$_2$-CH$_3$) 1.66 (m, 2H ButMA, –CH$_2$-CH$_2$-CH$_3$), 1.90 (s, 6H BIB, (CH$_3$)$_2$-C-CO-), 3.30 (m, 2H PHEA, –NHCH$_2$CH$_2$O–), 3.58 (m, 2H PHEA, –NHCH$_2$CH$_2$OH), 4.13 (m, 2H ButMA, (CO)-O-CH$_2$-CH$_2$-CH$_2$), 4.74 (m, 1H PHEA –NHCH (CO)CH$_2$–).

2.4. Synthesis of PHEA-g-BIB-pButMA-g-PEG-Biotin copolymer

The derivatization of PHEA-g-BIB-pButMA with biotin-dPEG®$_{11}$-NH$_2$ was performed by using the coupling agent bis(4-nitrophenyl) carbonate (BNPC). During the first step, 1 g of PHEA-g-BIB-pButMA (1.45 mmol of repeating units) was dissolved in 20 mL of aDMF, then 2.5 mL of a BNPC solution (24.4 mg mL^{-1} in aDMF) were added (molar

ratio between BNPC and repeating units equal to 0.08). The reaction mixture was left under stirring at 40 °C for 4 h. Later, 154.2 mg of biotin-dPEG®11-NH2 dissolved in 7.5 mL of aDMF were added to the flask. The mixture was maintained under stirring at 25 °C overnight and then dialyzed (MWCO 12–14 kDa) for two days against alkaline water (NaOH) and for another three days against ultrapure water. On completion, the solution was freeze-dried and stored for further characterization.

^{1}H NMR (300 MHz, DMF-d7, 25 °C, TMS) δ: 0.99 (m, 6H ButMA, –CH-CH$_3$ and –CH$_2$-CH$_2$-CH$_3$), 1.48 (m, 2H ButMA, –CH$_2$-CH$_2$-CH$_3$) 1.66 (m, 2H ButMA, –CH$_2$-CH$_2$-CH$_3$), 1.90 (s, 6H BIB, (CH$_3$)$_2$-C-CO-), 3.29 (m, 2H PHEA, –NHCH$_2$CH$_2$O–), 3.58–3.6 (m, 2H PHEA, –NHCH$_2$CH$_2$OH; m, 45H PEG, –OCH$_2$CH$_2$O–), 4.13 (m, 2H ButMA, (CO)-O-CH$_2$-CH$_2$-CH$_2$), 4.74 (m, 1H PHEA –NHCH(CO)CH$_2$–).

^{13}C NMR (400 MHz, DMF-d7, 25 °C, TMS): 177.43 (CO)$_{BIB}$, 172.07–170.74 (CO)$_{PHEA}$, 71.39 (–CH$_2$-O-)$_{PEG}$, 64.74 (–CH$_2$-O-)$_{ButMA}$, 60.09 (–CH$_2$-O-)$_{PHEA}$, 54.46 (–CH-CO)$_{PHEA}$, 45.77 (–CH$_2$-)$_{ButMA}$, 44.94 (–HN-CH$_2$-)$_{PHEA}$, 38.36 (–CH$_2$-CO)$_{PHEA}$, 19.5 (–CH$_3$)$_{ButMA}$, 13.61 (–CH$_3$)$_{ButMA}$.

2.5. Size exclusion chromatography

Weight average molecular weight (Mw) and polydispersity (PD) of each copolymer were determined by a size exclusion chromatography (SEC) analysis, performed using Phenomenex Phenogel 5 μm 104A columns connected to an Agilent 1260 Infinity Multi-Detector GPC/SEC system (Milan, Italy). Analyses were carried out at 50 °C in DMF+0.1 M LiBr as a mobile phase with a flow of 0.8 mL/min, performing absolute calibration of the instrument with a polystyrene standard (70 kDa).

2.6. Preparation of lenvatinib loaded nanoparticles

The preparation of nanoparticles involved the use of the pestle and mortar grinding method to ensure intimate contact between the drug and the polymeric matrix. In detail, 200 mg of polymer were mixed with 60 mg of lenvatinib mesylate and soaked with a solution of poly-vinylpyrrolidone in methanol/water 80:20 (100 mg in 10 ml), slowly dripped while stirring with the pestle. The entire mixture was processed for 15 min by grinding method until solvents evaporated. The resulting thin film was then rinsed with water and the colloidal dispersion obtained was finally filtered through 5 μm membrane filter (Sartorius, Minisart Syringe Filter, Germany) and freeze-dried. This process allowed to gain both non targeted (PBB-LEN) and biotinylated (PBB-BT-LEN) lenvatinib nanoparticles.

2.7. Dynamic light scattering (DLS) and zeta-potential measurements

The size distribution and Zeta-potential analyses were performed on 1 mL of nanoparticles dispersion in water at the concentration of 0.25 mg mL^{-1}. The mean hydrodynamic diameters were determined through dynamic light scattering (DLS) measurements using a Malvern Zetasizer NanoZS instrument equipped with a 632 nm laser and a fixed scattering angle of 173°. Z-average and PDI values were derived from the analysis of correlograms. DLS measurements were also performed to assess the stability of the nanoparticles overtime after storage at 4° C and 25° C, analyzing weekly the dispersions of the samples prepared as described above. The surface charge analyses were carried out through aqueous electrophoresis measurements at 25 °C, using the same instrument employed for the DLS measurements. Zeta-potential values (mV) were calculated from electrophoretic mobility using the Smoluchowski relationship.

2.8. Determination of nanoparticles drug loading and quantification of surface-exposed biotin

The drug loading of nanoparticles was quantified using Agilent 1260 Infinity high-performance liquid chromatography (HPLC), equipped with a multiple wavelength detector, operating at 240 nm, and an Open Lab Chemstation software. The elution was carried out isocratically at 25 °C, using a reverse-phase Gemini C6-phenyl 110A column (Phenomenex 5 μm, 250 × 4.60 mm) and methanol/water 85:15 mixture as a mobile phase with a flow rate of 1 mL min^{-1}. Nanoparticles were dissolved in a known amount of DMF and then methanol was added; the mixture was vigorously stirred for 3 h to extract the drug. The resulting suspension was centrifuged (14500 rpm for 10 min at 25 °C), filtered through syringe filter (0.2 μm cut-off) and 50 μL of the resulting solution were injected. The chromatograms were analyzed quantifying the drug amount loaded into the nanoparticles with a calibration curve obtained with lenvatinib mesylate standards in mobile phase (0.5–100 μg mL^{-1}). The drug loading (DL%) was expressed as the weight percent ratio between the loaded drug and the freeze-dried nanoparticles.

To quantify the amount of biotin exposed on the nanoparticles surface, available for receptor recognition, the HABA-avidin colorimetric assay was performed. Specifically, PBB-BT were dispersed at a concentration of 1 mg mL^{-1} in ultrapure water and incubated with the HABA-avidin reagent following the manufacturer's instructions. UV readings were taken on filtered samples (syringe filter, cut-off 0.2 μm), and the amount of biotin was expressed as mol/mol percentage with respect to the repeating units of the copolymer.

2.9. Thermal analysis

PBB-BT-LEN and PBB-LEN were also analyzed by differential scanning calorimetry (DSC) coupled with thermal gravimetric analysis (TGA), using a DSC/TGA 131 EVO (by SETARAM Instruments). Each measurement was performed under nitrogen atmosphere with a flow of 1 mL min^{-1}, using about 5 mg of dried sample placed into an alumina crucible. Samples were heated starting from 20 °C up to 500 °C, with a heating rate of 10 °C min^{-1}.

2.10. Raman analysis

Raman spectra analysis was carried out by using a Horiba iHR550 Spectrometer, which was coupled to an Olympus microscope BX53M and equipped with a Super-Head for selecting the 473 nm laser line (solid state COBOLT). The setup featured a 600 lines/mm diffraction grating and was linked to a Horiba Syncerity CCD detector. The acquisition of Raman spectra involved focusing 3 mW of the exiting laser line through a 50X LWD (long working distance) objective with NA=0.9, for a duration of 40 s. Several spectra were acquired at various points on each sample to allow a more accurate statistical analysis. Subsequently, data analysis and the removal of fluorescence backgrounds were performed by using the LabSpec software developed by Horiba.

2.11. Drug release studies

For drug release experiments, a proper amount of PBB-BT-LEN or PBB-LEN (corresponding to 0.125 mg of lenvatinib mesylate) were dispersed in 1 mL of water and placed into a dialysis tubing (12–14 kDa cut-off). The external media (9 mL) were chosen to mimic two different administration routes. Specifically, DPBS pH 7.4 was used to mimic an intraperitoneal administration, while the oral administration was simulated by using 0.1 M HCl for 2 h and PBS pH 6.8 for further 22 h. At fixed time intervals, 0.2 mL of the receiving compartment was withdrawn and replaced with equal volume of fresh medium. The experiment was stopped after 24 h and the drug released was quantified using HPLC analysis as described above.

2.12. In vitro studies

2.12.1. Cell culture

Human hepatocellular carcinoma cell line (HepG2) was purchased

from the American Type Culture Collection (ATCC, Rockville, MD, USA). HepG2 were grown in Eagle's modified minimum essential media (EMEM) supplemented with 10 % fetal bovine serum (FBS, Life Technologies, Gibco®; Carlsbad, CA, USA) and 1 % penicillin–streptomycin (Sigma-Aldrich, St. Louis, MO, USA). Cells were maintained at 37 °C in an incubator under 5 % CO2. Cells were cultured about 80 % of confluents in T-75 flasks and the media were changed one additional time a week.

2.12.2. Cell viability assay

To evaluate cell viability, a 3-(4,5-dimethylthiazol-2-yl)-5-(3-carboxymethoxyphenyl)-2-(4-sulfophenyl)–2H-tetrazolium (MTS) inner salt assay was used as previously described (Giammona et al., 2022b). HepG2 cells were plated on 96-well plates at a density of 4×10^4 cells/well to a final volume of 150 μL. After 24 h, cells were treated with PBB-BT-LEN, PBB-LEN, and free LEN, corresponding to lenvatinib mesylate concentrations of 1 μM, 2.5 μM, 5 μM, 7.5 μM, 10 μM and 15 μM. After 24, 48, or 72 h of incubation with the test compounds, the cells were washed twice with Dulbecco's phosphate-buffered saline (DPBS) pH 7.4, and 120 μL of MTS assay solution diluted 6 times in MEM was added to each well. The cells were then incubated for 4 h at 37 °C and 5 % CO_2 before reading the absorbance at 492 nm using a microplate reader. Cell viability was expressed as a percentage of living cells compared to the untreated control of seeded cells (taken as 100 %). The cytotoxic effect of the lenvatinib-loaded in biotinylated and non-biotinylated nanoparticles was compared with that of free drug and empty nanoparticles at equivalent concentrations. All experiments were performed in triplicate.

2.13. In vivo studies

2.13.1. Animals

Male C57BL/6J wild-type nude mice (25–30 g; 4–6 weeks of age) were obtained from Jackson Laboratory (Bar Harbor, Hancock, ME, USA) and kept in a room at 22 ± 1 °C having pathogen-free micro-isolator cages as well as a 12-hour light/12-hour dark cycle for a week. Mice were fed with standard diet and had unlimited access to micro-filtered water. This study was performed following Italian regulations on the use of animals (D.M.116192) and Directive legislation (EU) (2010/63/EU) amended by Regulation (EU) 2019/1010.

2.13.2. Xenograft model of hepatocellular carcinoma (HCC)

The xenograft HCC model was performed as previously indicated (Cervello et al., 2017), in order to demonstrate drug proof-of-principle. The ectopic model was carried out by subcutaneous inoculation, in the right flank of each mouse, with 10×10^6 human HCC HepG2 cells in 0.2 mL of phosphate buffered saline (PBS) and 0.1 mL matrigel (BD Bioscience, Bedford, MA, USA). After tumor induction, animals were monitored daily for morbidity and mortality. Then, 21 days from inoculation, when the tumor reached a modest volume of around 300 mm³, the animals were randomly divided into various experimental groups and treated daily for 3, 7 and 18 days, both via oral and intraperitoneal administration, as follows:

Group 1: CTR: mice subjected to xenograft HCC model and then treated with vehicle solution (N=60; 30 for ip administration and 30 for os administration);

Group 2: PBB: mice subjected to xenograft HCC model and then treated with PBB (N=60; 30 for ip administration and 30 for os administration);

Group 3: PBB-BT: mice subjected to xenograft HCC model and then treated with PBB-BT (N=60; 30 for ip administration and 30 for os administration);

Group 4: LEN: mice subjected to xenograft HCC model and then treated with free LEN (N=60; 30 for ip administration and 30 for os administration);

Group 5: PBB-LEN: mice subjected to xenograft HCC model and then treated with PBB-LEN (N=60; 30 for ip administration and 30 for os administration);

Group 6: PBB-BT LEN: mice subjected to xenograft HCC model and then treated with PBB-BT LEN (N=60; 30 for ip administration and 30 for os administration).

Groups 4, 5 and 6 have received doses corresponding to 10 mg kg⁻¹ of lenvatinib, while groups 2 and 3 have received the equivalent dose of drug free nanoparticles.

For intraperitoneal or oral administration, lenvatinib was dissolved in a solution of DMSO 10 % and saline 90 %, while other formulations were dispersed in saline only. Doses and the route of administration used in this study were based on previous in vivo studies (Cervello et al., 2017; Ogasawara et al., 2019). At the respective three time-points (3-, 7- and 18-days of treatment) mice were sacrificed, tumors were surgically excised and processed for histological examinations or biochemical analyses. Furthermore, to carry out biodistribution studies, the spleen, liver, and kidneys of each experimental group were collected.

#### 2.13.3. Histological evaluation and tumor burden measurement

For histological evaluation, tumors were removed, fixed for 24 h at 25 °C in a 10 % (w/v) PBS-buffered formaldehyde solution, dehydrated with graded ethanol, and embedded in paraffin. Then, the obtained 7 μm thick sections were stained with hematoxylin and eosin (H&E) to investigate tissue morphology as previously specified (Filippone et al., 2022). Tumor samples were evaluated by using a 0–5-point scale that referred to several parameters such as marked hypercellularity, nuclear atypia, microvascular proliferation, and necrosis (0 = no tumor spreading, 1 = poor tumor differentiation, 2 = moderate differentiation and nuclear atypia, 3 = differentiated tumor cells, 4 = well defined nuclear atypia and spreading, 5 = extreme spreading) as previously reported (Filippone et al., 2022). A Nikon Eclipse Ci-L microscope was used to acquire the images, that were showed at a magnification of 20× (50 μm scale bar). The extent of tumor burden is an important concern in treatment selection for HCC and total tumor volume is considered an independent and better prognostic marker to indicate tumor burden in HCC patients (Ho et al., 2023; Lee et al., 2013). Therefore, following animals' sacrifice (at 3, 7 and 18 days), tumor volumes were measured by using an electronic caliper in order to obtain tumor burden measure. Specifically, the tumor burden was calculated using the following formula: 0.5 × length × width (Scuderi et al., 2021).

2.13.4. Immunohistochemical analysis of cluster of differentiation 34 (CD34) and vascular endothelial growth factor (VEGF)

Immunohistochemical analysis was executed as previously described (Ardizzone et al., 2022). Briefly, tumor sections were deparaffinized, rehydrated and then incubated overnight (O/N) with the following primary antibodies: anti-VEGF (Santa Cruz Biotechnology, Dallas, TX, USA; 1:100 in PBS, v/v; sc-7269) and anti-CD34 (1:100; Santa Cruz Biotechnology, Dallas, TX, USA; sc-74499). Sections were washed with PBS and incubated with the secondary antibody using the VECTASTAIN Universal Quick Kit, Peroxidase, R.T.U. (PK-7800; Vector Laboratories, Burlingame, CA, USA). The chromogenic substrate 3,3′-Diaminobenzidine (DAB) was used to reveal the immunohistochemical reaction, and Nuclear Fast Red was used as a counterstain. Using a Nikon Eclipse Ci-L microscope, blinded observations of immunohistochemical pictures were made with Image J software, while GraphPad version 8.0 (La Jolla, CA, USA) was used to create the histogram and perform the statistical analysis. Images are shown at 20× (50 μm scale bar).

2.13.5. Immunofluorescence analysis of p53 apoptosis marker

The immunofluorescence analysis was performed as described previously (Filippone, A., et al.,2021). Tumor tissue sections of 7 μm thick were deparaffinized and placed in 0.1 M citrate buffer for one minute, permeabilized in 0.2 % Triton X-100/PBS and blocked with 10 % bovine albumin serum (BSA). Then sections were incubated with anti-p53 primary antibody (1:100; sc-126; Santa Cruz Biotechnology, Dallas, TX,
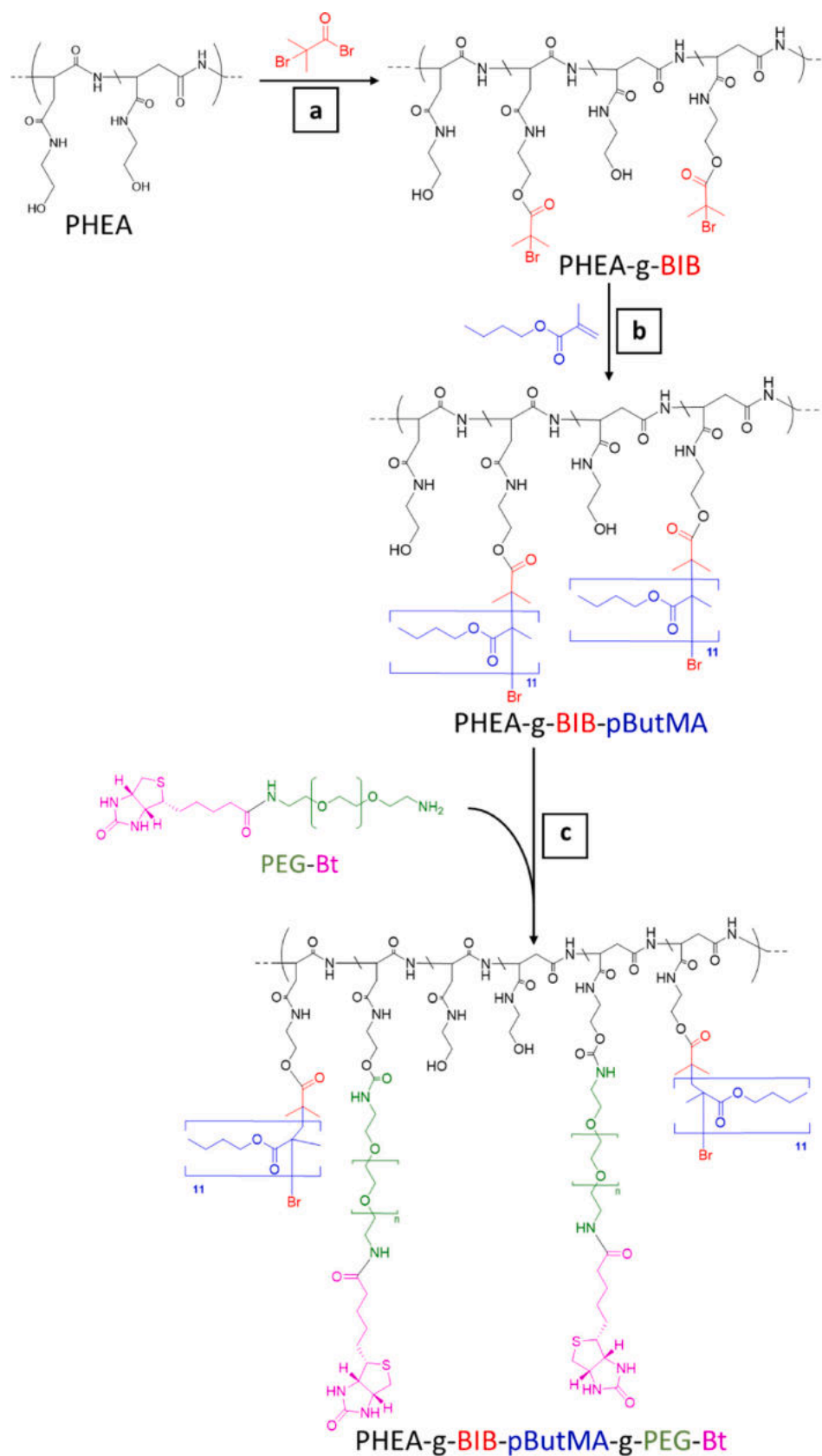
Scheme 1. Synthetic pathway of PHEA-g-BIB-pButMA-g-PEG-Bt. a) starting condition aDMA, TEA, 0 °C, 15 min, then RT, 4 h b) Ar atm, aDMF/MeOH, Cu^I Br, Bpy, 50 °C, 20 h. c) starting condition aDMF, BNPC, 40 °C, 4 h, then 25 °C, overnight.

USA) overnight in a humidified chamber at 37 °C. Subsequently, the sections were washed with PBS and incubated with secondary antibody, a fluorescein-isothiocyanate (FITC)-conjugated anti-mouse Alexa Fluor-488 antibody (1:1000 v/v Molecular Probes, Altrincham, UK), for 3 h at room temperature. Finally, sections were washed and 2 µg/mL 4′,6′-diamidino-2-phenylindole (DAPI; Hoechst, Frankfurt; Germany) in PBS was added for nuclear staining. Sections were observed and acquired at 40 × magnification using a Nikon Eclipse Ci-L microscope.

2.13.6. Western blot analysis of BCL2 associated X protein (Bax) and B cell lymphoma-2 (Bcl-2)

Analysis of Bax and Bcl-2 markers has been performed using western blot (Campolo et al., 2021). Firstly, tumor samples were homogenized in order to extract the cytosolic and nuclear fractions. Later, using bovine serum albumin (BSA) as standard, a Bio-Rad protein assay was utilized to determine the amount of protein in each sample. Subsequently, samples were heated at 95 °C for 5 min, loaded on a 10 % SDS-PAGE gel and transferred to a polyvinylidene difluoride (PVDF) membrane. Following this step, the membranes were blocked for one hour at room temperature using 5 % (w/v) nonfat dry milk in buffered saline. Membranes were incubated O/N with the following primary antibodies: anti-Bax (1:500; Santa Cruz Biotechnology, Dallas, TX, USA; sc-7480); and anti-Bcl-2 (1:500; Santa Cruz Biotechnology, Dallas, TX, USA; sc-7382) in 1 × PBS, 5 % (w/v), non-fat dried milk, and 0.1 % Tween-20. Afterward, membranes were washed and incubated with a secondary antibody, anti-mouse (1:10000, Jackson ImmunoResearch, West Grove, PA, USA) for 1 h at room temperature. Moreover, to ensure that the samples had the same amount of proteins, membranes were incubated with anti-β-actin primary antibody (1:500; sc-47778; Santa Cruz Biotechnology, Dallas, TX, USA).

2.13.7. Enzyme-Linked immunosorbent assay (ELISA) assay

ELISA kits were used to detect the levels of Ki-67 (MyBiosource, cat. No. MBS1601117), caspase-3 (MyBiosource, catalog No. MBS849298), caspase-8 (LifeSpan Bioscience, Inc. catalog. No. LS-F32785) and caspase-9 (LifeSpan Bioscience, Inc. catalog. No. LS-F21324) in tumors tissue homogenates as previously described (Ardizzone et al., 2023), and according to the manufacturer's protocols.

2.13.8. Biodistribution studies

To quantify the amount of drug accumulated in mice organs after 18 days of treatment, lenvatinib was extracted from the explanted organs (liver, spleen, kidney and tumor). Specifically, each organ sample was washed in 0.9 % NaCl, mixed with TRIS buffer (2 mL, 1 M, pH 8) in a 15 mL glass tube and homogenized using an Ultraturrax T 25 (Janke&Kunkel ka − Labortechnik). Methanol (1 mL) was then added to precipitate the proteins. The homogenized samples were thus extracted three times with dichloromethane (2 mL), followed by centrifugation (4000 rpm, 5 min, room temperature). The organic phases were transferred into a glass tube and evaporated to dryness. Each dried residue was then retrieved with a mixture of methanol/water (70:30) (0.6 mL), filtered through a 0.22 µm syringe filter and a volume of 50 µL was injected into the HPLC system described above; the chromatographic procedure was carried out isocratically at 25 °C, using a reverse-phase Gemini C6-phenyl 110A column (Phenomenex 5 µm, 250 × 4.60 mm), methanol/water 70:30 as a mobile phase at a flow rate of 1 mL min⁻¹.

2.14. Statistical analysis

All values are reported as mean ± standard deviation (SD) of "N" observations. The results were analyzed by One-Way analysis of variance (ANOVA) followed by a Bonferroni post-hoc test for multiple comparisons. Only a p-value less than 0.05 ($p < 0.005$) was considered significant.

Table 1
Values of weight average molar weight (Mw) and polydispersity (Mw/Mn) determined through SEC analysis and molar derivatization degrees (DD %) calculated by ^{1}H NMR analyses.

Derivative	$\overline{M}_w$	$\overline{M}_w/\overline{M}_n$	DD$_{BIB}$%	DD$_{ButMA}$%	DD$_{PEG}$%
PHEA	45,446	1.4	–	–	–
PHEA-g-BIB	67,192	1.7	35	–	–
PHEA-g-BIB-pButMA	399,098	1.9	35	385	–
PHEA-g-BIB-pButMA-g-PEG-Bt	427,398	2.0	35	385	7

3. Results and discussion

### 3.1. Polymer synthesis and characterization

Aiming to produce nanoparticles for the effective drug delivery of the emerging drug lenvatinib, the first step was the design and synthesis of a polymeric derivative through controlled polymerization. In this regard, Atom Transfer Radical Polymerization (ATRP) has been chosen since it is highly suitable for the tailored synthesis of polymers with well-defined structures and functionalities, crucial for biomedical applications. Prior research has shown that the synthesis of amphiphilic brush copolymers consisting of PHEA as hydrophilic backbone and hydrophobic poly-butylmethacrylate pendant groups by ATRP, has led to the development of polymeric nanosystems with noteworthy efficacy in hepatocarcinoma drug delivery (Cervello et al., 2017). Thus, the potentialities of this copolymer were enhanced by conjugating biotin as a targeting agent to boost the selectivity of hepatocarcinoma treatment. The synthesis of the graft copolymer PHEA-gBIB-(pButMA)-g-PEG-Bt involved three sequential steps. In the initial stage, PHEA underwent derivatization with 2-bromoisobutyryl bromide (BIBB) residues taking advantage of the reactivity of hydroxyl groups toward acyl bromide, catalyzed by triethylamine. The degree of derivatization in BIB achieved was determined as 35 mol%, calculated via ^{1}H NMR analysis by comparing the integral of the peak corresponding to the methyl groups at δ 1.95 of BIB with that assigned to CH$_2$ of the PHEA backbone at δ 3.29 ppm (Figure S1). The resulting multifunctional macroinitiator was then employed as a starting material for Atom Transfer Radical Polymerization (ATRP) of the hydrophobic monomer butyl methacrylate (ButMA), constituting the second step of the synthesis pathway. The analysis of the ^{1}H NMR spectrum of the obtained brush copolymer revealed a derivatization degree in ButMA of 385 mol%, calculated by comparing the integral of the peak corresponding to the methyl groups at δ 0.99 of ButMA with that assigned to CH$_2$ of the PHEA backbone at δ 3.30 ppm (Figure S2). Considering the previously calculated derivatization degree in BIB as 35 mol%, the polymerization extension (n) of ButMA was determined to be 11 (n = derivatization degree in ButMA/derivatization degree in BIB). In the final synthetic phase, the graft copolymer PHEA-g-BIB-pButMA was further functionalized with biotinylated polyethylene glycol via carbonate ester, allowing the formation of a carbamate linkage between the free amino group of the pegylated targeting agent and the hydroxyl group of the PHEA backbone. The ^{1}H NMR spectrum of the new targeted copolymer PHEA-g-BIB-pButMA-g-PEG-Bt was used to calculate the derivatization degree in PEG, resulting in 7 mol% by comparing the integral of the peak corresponding to the methylene groups at δ 3.58 of PEG with that assigned to CH$_2$ of the PHEA backbone at δ 3.29 ppm (Figure S3). Furthermore, ^{13}C NMR spectrum confirmed the successful functionalization, as observable from the appearance of the peak at δ 71.39 ascribable to the presence of polyethylene glycol (Figure S4). Scheme 1 shows the synthetic pathway of PHEA-g-BIB-pButMA-g-PEG-Bt.

All the obtained copolymers were characterized by SEC analysis in terms of weight average molar weight (Mw) and polydispersity (Mw/Mn) and the obtained values are reported in Table 1. The data led to an increase in molecular weight consistent with the sequential

Table 2
Characterizations of the nanoparticles. Size, polydispersity index (PDI), surface charge and drug loading of lenvatinib nanoparticles.

	Z-Average (nm)	*PDI*	Z-Potential (mV)	Drug Loading (% w/w)
PBB-LEN	392.7 ± 47	0.35 ± 0.15	−18.0 ± 4.8	13.2 ± 1.3 %
PBB-BT-LEN	393.8 ± 26	0.340 ± 0.18	−22.6 ± 4.6	11.4 ± 1.5
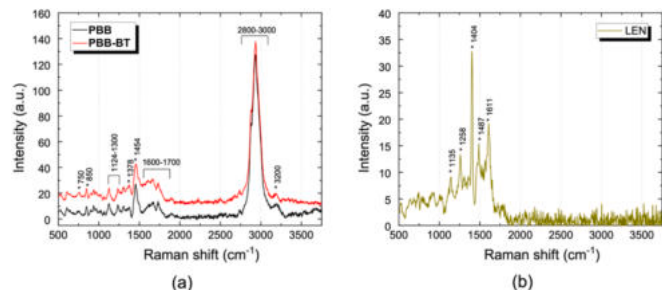
Fig. 1. (a) Raman spectra of PBB (black line) and PBB-BT (red line); (b) Raman spectrum of Lenvatinib in powder form (dark-green line). The asterisks mark the center-frequencies of the vibrational modes for identification.

derivatizations performed.

3.2. Preparation and characterization of lenvatinib loaded polymeric nanoparticles

To identify the method that leads to the optimal combination of desirable size, stability in an aqueous medium, and high drug content for nanoparticles, different preparation techniques were explored. The most favourable outcomes were achieved through the mortar-pestle grinding technique (Figure S5). The nanoparticles loaded with lenvatinib were examined using dynamic light scattering (DLS) to assess both size distribution and zeta potential. The weight percentages of entrapped drug were determined through HPLC analysis. A summary of all characterizations is provided in Table 2.

Both lenvatinib loaded nanoparticles exhibited almost overlapping size and surface charge indicating that the conjugation with PEG-Bt does not exert a significant influence on these basic parameters. In a similar manner, the drug payloads calculated appeared comparable in both cases, showing the lenvatinib was successfully incorporated into the nanosystems. These results suggest that the nanoparticles formulated might be able to deliver efficiently this antineoplastic drug to the tumor target.

The analysis of the biotin content exposed on the nanoparticles' surface and thus available for receptor interaction resulted equal to 1.5 % mol/mol% compared to the repetitive units of the copolymer. Furthermore, stability studies performed by DLS analyses up to 1 month,

revealed that the loaded nanoparticles maintain almost unaltered characteristics after storage as lyophilized powder at 4° C or 25 °C (Table S1).

DSC analyses (Figures S6-S7) suggested that lenvatinib is presumably entrapped into nanoparticles as a molecular dispersion, since it was not possible to clearly distinguish the peaks related to the fusion of the free drug after incorporation. In Fig. 1(a) the Raman spectra of PBB (black line) and PBB-BT (red line) within the 500 cm^{-1} to 3750 cm^{-1} range are reported following the fluorescence background removal. Both spectra predominantly exhibit vibrational signals from PVP, with discernible contributions from the PBB amino groups in the spectral region between 1600 cm^{-1} and 1700 cm^{-1}. Despite examining the spectra profile, it is not possible to distinguish differences between the non-biotinylated NPs (PBB) and the biotinylated counterparts (PBB-BT). Fig. 2(b) shows the Raman spectrum of Lenvatinib powder after subtraction of the fluorescence background, which is introduced by the laser excitation. The very bright fluorescence intensity, especially at higher Raman frequencies, obscures the –CH stretch signals in the region between 2800 cm^{-1} and 3300 cm^{-1} (refer to figure S8). Despite the pronounced fluorescence of the sample, a discernible contribution of the Raman fingerprint is evident from 500 cm^{-1} to 2000 cm^{-1}.

The tentative vibrational assignments of NPs, biotinylated and not, and of Lenvatinib powder spectral contributions are reported in Table 3 and 4, respectively.

*Legend: ν = stretching; β = bending; δ = in plane bending; γ = out of

Table 3
Raman peaks assignment of PBB and PBB-BT (Borodko et al., 2006).

PBB and PBB-BT Raman frequency shift	
Frequency (cm^{-1})	**Mode assignment***
750	C–C chain
850	C–C ring
1124	C–C, $\rho(CH_2)$
1300	$\omega(CH_2)$, $\nu(N–H)$
1378	$\beta(C–H)$
1500	C-N
1665	$\nu(C=O)$, $\nu(C-N)$
2877	$\nu(C–H)$
2900–3000	$\nu_{sym}(C–H)$ ring, $\nu_{sym}(CH_2)$, $\nu_{as}(C–H)$ ring, $\nu_{as}(CH_2)$

Table 4
Raman peaks assignment of Lenvatinib powder.

Lenvatinib Raman frequency shift	
Frequency (cm^{-1})	**Mode assignment***
1135	$\delta(C–H)$ in benzene rings, $\nu(C-N)$, $\omega(C–H)$ in CH_3
1258	$\nu(C-N)$, $\nu(C–C)$, $\delta(C–H)$, $\delta(N–H)$
1404	$\nu(C–C)$ benzene ring
1487	$\nu(C–C)$, $\delta(C–H)$ benzene ring, $\delta(N–H)$
1611	$\nu(C=C)$ benzene, $\delta(N–H)$, $\delta(C–H)$ benzene
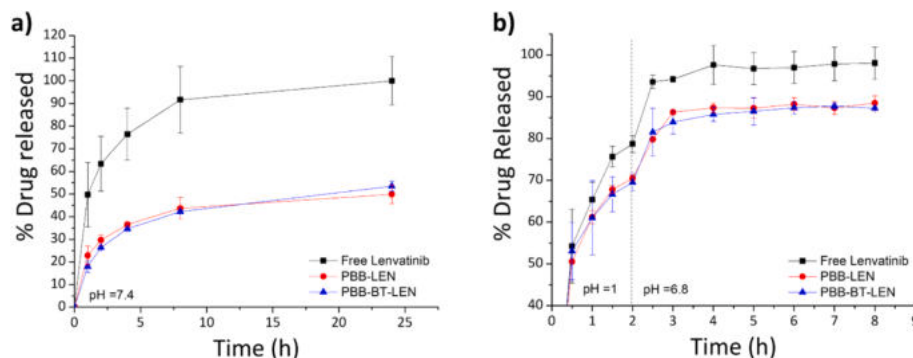
Fig. 2. Drug release profiles of PBB-LEN and PBB-BT-LEN mimicking parenteral administration (a) or oral administration (b).
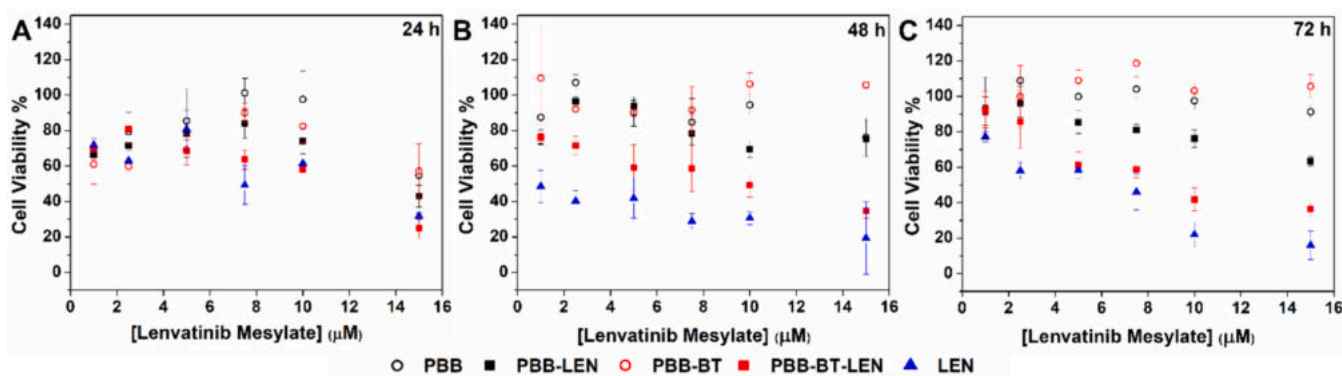
Fig. 3. Cell viability assay on HepG2 cells after 24 h (A), 48 h (B) and 72 h (C) of treatment with PBB, PBB-BT, PBB-LEN, PBB-BT-LEN and LEN.

plane bending; ω = wagging; ρ = rocking.

*Legend: ν = stretching; β = bending; δ = in plane bending; γ = out of plane bending; ω = wagging; ρ = rocking.

When the nanoparticles are loaded with the Lenvatinib drug, the fluorescence contribution is so substantial that distinguishing any Raman peak becomes challenging, even after the removal of the fluorescence background (Figure S8).

3.3. Drug release studies

The ability of nanoparticles to release the entrapped drug in a controlled manner was assessed under physiological conditions, simulating intraperitoneal administration (pH 7.4 at 37 °C, 24 h) or oral administration (pH 1 at 37 °C, 2 h; pH 6.8 at 37 °C, 22 h). As shown in Fig. 2, unlike the free drug, the nanoparticles allow a slow and sustained drug release over time under physiological conditions, releasing about 50 % of the entrapped drug in 24 h without recording any potentially problematic burst effect. At the same time, no significant difference is shown by the presence of PEG on the surface of the nanoparticles. A different profile is observed under conditions that mimic oral administration. In a highly acidic environment (pH 1), a consistent burst effect is observed, as approximately half of the drug content is released in the first 30 min. Subsequently, a gradually decreasing drug release is registered until an almost static condition is reached after the first 3 h, i. e. after the pH change. This behavior results from the different solubility of lenvatinib in an acidic environment due to the presence of a quinoline-type aromatic heterocycle with alkaline properties in its chemical structure.

3.4. In vitro studies

Cytotoxicity studies after PBB e PBB-BT treatments, showed a lack of efficacy on the HepG2 cell line by recording high percentages of cell viability (Fig. 3 panels A-C). Furthermore, 24 h treatments with LEN and PBB-BT-LEN showed a significant cytotoxic effect at the concentration of 7.5 μM, 10 μM and 15 μM compared to the control cells (Fig. 3 panel A). After 48 h of treatment with PBB-BT-LEN and LEN a significant reduction of cell viability was observed at the concentrations of 5 μM, 7.5 μM, 10 μM and 15 μM (Fig. 3 B). Greater efficacy in reducing cell viability was observed after 72 h of treatments with PBB-BT-LEN and LEN (10 μM and 15 μM) compared to the control cells (Fig. 3 panel C). In addition, also PBB-LEN partially decreased cell viability compared to the control group, even if less considerably respect LEN or PBB-BT-LEN (Fig. 3 panels A-C). Overall, these data highlight the cytotoxic effect of PBB-BT-LEN.

3.5. In vivo efficacy

3.5.1. Efficacy of treatment with PBB-LEN and PBB-BT LEN in reducing tumor burden, histological damage, and Ki-67 levels

To evaluate the in vivo efficacy of targeted nanoparticles, a HepG2 xenograft model was used as it allows a rapid and efficient investigation of the in vivo fate of a compound in a pre-clinical trial. Firstly, we evaluated the effectiveness of 3 days of treatment with PBB, PBB-BT, PBB-LEN, PBB-BT-LEN and LEN through histological and molecular biology analyses. After 3 days of treatments, histological analyses as well as mean tumor burden and Ki-67 evaluations revealed that both oral and intraperitoneal administrations of all compounds were ineffective in reducing tumor features compared to the CTR group (Figure S9). Similarly, Western blot analysis and ELISA kits showed no significant differences in the expression of pro-apoptotic proteins Bax and Caspase −3, −8 and 9 as well as the anti-apoptotic protein Bcl-2 compared to CTR animals (Figure S10). Furthermore, immunofluorescence analysis demonstrated that all treatments, both oral and intraperitoneal, did not increase the number of p53 positive cells compared to the CTR group (Figure S10). We also detected the expression of angiogenic factors such as VEGF and CD34 by immunohistochemistry analysis. Our data revealed that 3 days of oral or intraperitoneal treatments with PBB, PBB-BT, LEN, PBB-LEN, PBB-BT-LEN did not reduce the number of positive cells positive for both CD34 and VEGF compared to CTR mice (Figure S11 and S12, respectively). Together these results highlight that following the 3 days of treatments with LEN, PBB-LEN and PBB-BT-LEN, administered orally or intraperitoneally, there was no statistically significant variation for all the parameters evaluated (tumor mass, infiltrative neutrophils, modulation of angiogenic and apoptotic markers as well as in the reduction of the proliferation marker Ki-67). After 7 days of both oral and intraperitoneal treatments with LEN, PBB-LEN and PBB-BT-LEN a significant reduction in histopathological score was observed compared to CTR animals (Figure S13). While no significant reduction was observed between LEN and PBB-LEN or PBB-BT-LEN systems (Figure S13). Similar results were observed when examining tumor burden and levels of the tumor marker Ki-67 (Figure S13). The obtained data demonstrated that treatment with LEN, PBB-LEN and PBB-BT-LEN significantly reduced tumor burden and Ki-67 levels compared to the CTR group, while no significant differences were detected between the administrations of LEN and LEN nanoparticles formulations PBB-LEN and PBB-BT-LEN (Figure S13). As well, the study of apoptotic markers demonstrated that oral or intraperitoneal treatments with LEN, PBB-LEN and PBB-BT-LEN were able to increase the expression of pro-apoptotic proteins such as Bax, Caspase-3, −8 and −9 while reducing Bcl-2 expression compared to the CTR group (Figure S14). However, no statistically significant difference was observed comparing LEN treatment with PBB-LEN or PBB-BT-LEN systems (Figure S14). Also, after 7 days of oral and intraperitoneal treatments, tumor tissue sections were subjected to immunohistochemical analysis for the evaluation of the
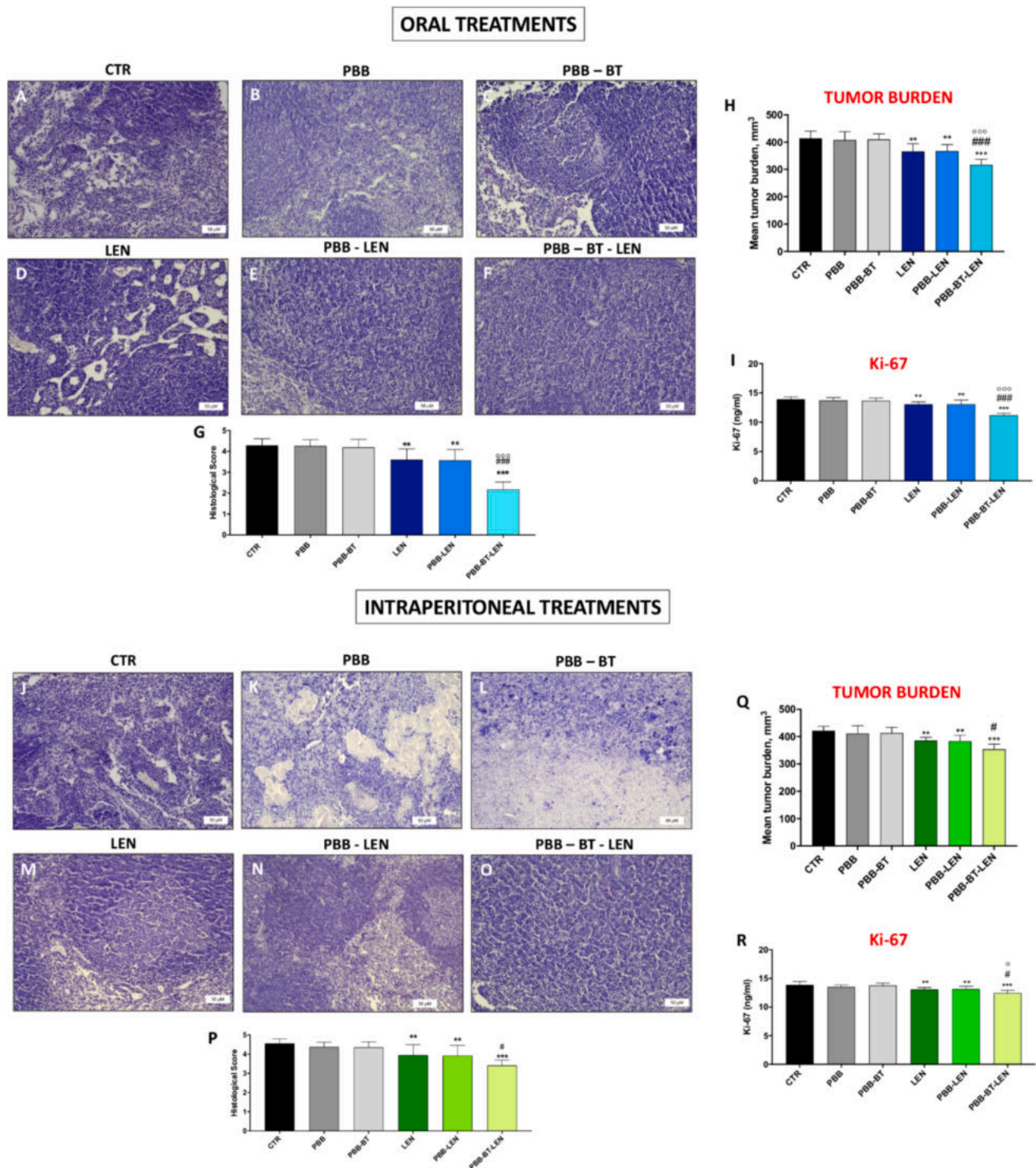
Fig. 4. Histological analysis, tumor burden and Ki-67 evaluations following 18 days of treatments. (A-F) Representative images of tumors following oral treatments (A) CTR groups, (B) PBB, (C), PBB-BT, (D) LEN, (E) PBB-LEN, (F) PBB-BT-LEN. (G) Histological score. (H) Tumor burden analysis for each experimental group after oral treatments. (I) ELISA assay result of Ki-67 after oral treatments. (J-O) Representative images of tumors following intraperitoneal treatments (J) CTR group, (K) PBB, (L) PBB-BT, (M) LEN, (N) PBB-LEN, (O) PBB-BT-LEN. (P) Histological score. (Q) Tumor burden analysis for each experimental group after intraperitoneal treatments. (R) ELISA assay result of Ki-67 after intraperitoneal treatments. Figures are shown at 20 × magnification. Values are means ± SD. One-way ANOVA test. ** $p < 0.01$ vs CTR; *** $p < 0.001$ vs CTR; # $p < 0.05$ vs LEN; ### $p < 0.001$ vs LEN; ° $p < 0.05$ vs PBB-LEN; °° $p < 0.01$ vs PBB-LEN. The scale bar represents 50 μm.

angiogenic factors such as CD34 and VEGF. The results obtained showed that animals treated, both orally and intraperitoneally, with LEN, PBB-LEN and PBB-BT-LEN significantly reduced the angiogenic markers CD34 and VEGF compared to the CTR group (Figure S15 and 16, respectively). Nevertheless, no significant differences were highlighted

between LEN-nanosystems (PBB-LEN and PBB-BT-LEN) and LEN administrations (Figure S15 and 16, respectively). After 18 days of oral administrations, tumor tissue was evaluated by H/E staining. Histological analysis showed that CTR groups, PBB and PBB-BT groups were characterized by morphological alteration of the tumor tissue, as high

ORAL TREATMENTS

INTRAPERITONEAL TREATMENTS
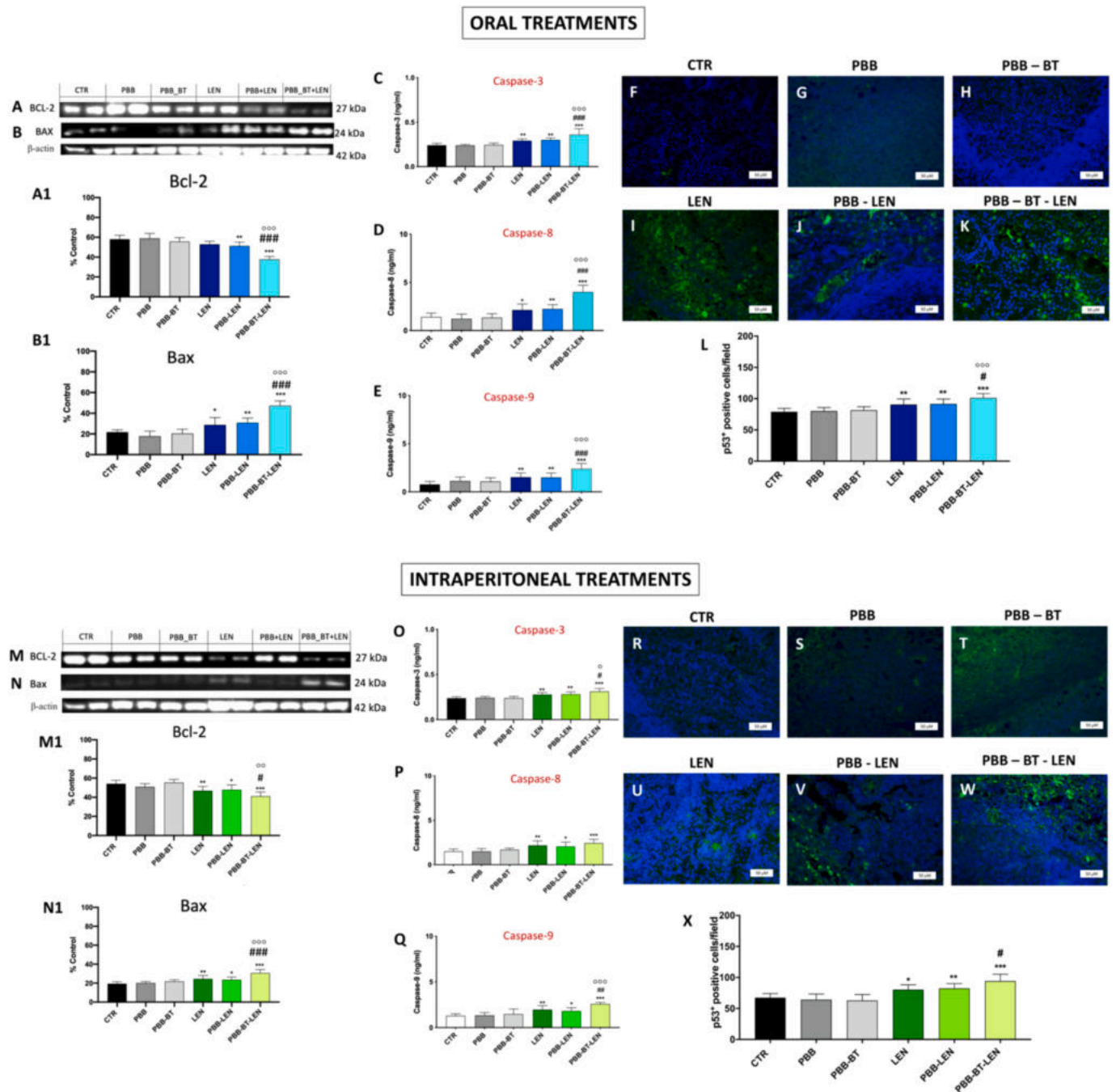
Fig. 5. Western blot analysis of apoptotic markers Bax and Bcl-2 and ELISA assay of Caspase 3, 8 and 9. (A–B) Representative blots of Bcl-2 and Bax after 18 days of oral administrations of LEN formulations (densitometric analysis A1–B1). (C-E) ELISA assay results of Caspase 3, 8 and 9 levels after 18 days of oral treatment with LEN formulations. (F-K) Representative images of immunofluorescence analysis following oral treatments (F) CTR group, (G) PBB, (H) PBB-BT, (I) LEN, (J) PBB-LEN, (K) PBB-BT-LEN. (L) Histological score (M–N). Representative blots of Bcl-2 and Bax after 18 days of intraperitoneal administration of different drug. (O-Q) ELISA assay results of Caspase 3, 8 and 9 levels after 18 days of intraperitoneal treatment with LEN formulations (densitometric analysis M1–N1). (R-W) Representative images of immunofluorescence analysis following intraperitoneal treatments (R) CTR group, (S) PBB, (T) PBB-BT, (U) LEN, (V) PBB-LEN, (W) PBB-BT-LEN. (X) Histological score. Images are shown at 40 × magnification. Values are means ± SD. One-way ANOVA test. * $p < 0.05$ vs CTR; ** $p < 0.01$ vs CTR; *** $p < 0.001$ vs CTR; # $p < 0.05$ vs LEN; ##$p < 0.01$ vs LEN; ### $p < 0.001$ vs LEN; ° $p < 0.05$ vs PBB-LEN; °° $p < 0.01$ vs PBB-LEN; °°° $p < 0.001$ vs PBB-LEN. The scale bar represents 50 μm.

neutrophilic infiltration (Fig. 4 panels A-C, histological score G). Oral administrations of LEN, PBB-LEN and PBB-BT-LEN were able to reduce the progression of the tumor mass and the infiltration of neutrophils compared to CTR group (Fig. 4 panels D-F, histological score G). Notably, the achieved results demonstrated that oral treatment with PBB-BT-LEN (Fig. 4 panel F, histological score G) reduced histological damage more effectively than treatment with LEN (Fig. 4 panel D,

histological score G) and with PBB-LEN (Fig. 4 panel E, histological score G). The evaluation of tumor burden revealed a notable reduction after oral treatments with LEN, PBB-LEN and PBB-BT-LEN compared to CTR group (Fig. 4 panel H). However, a marked significant reduction in tumor burden was obtained after oral administration with PBB-BT-LEN compared to free LEN and PBB-LEN administration (Fig. 4 panel H). To further study the effect of PBB-LEN and PBB-BT-LEN on cell
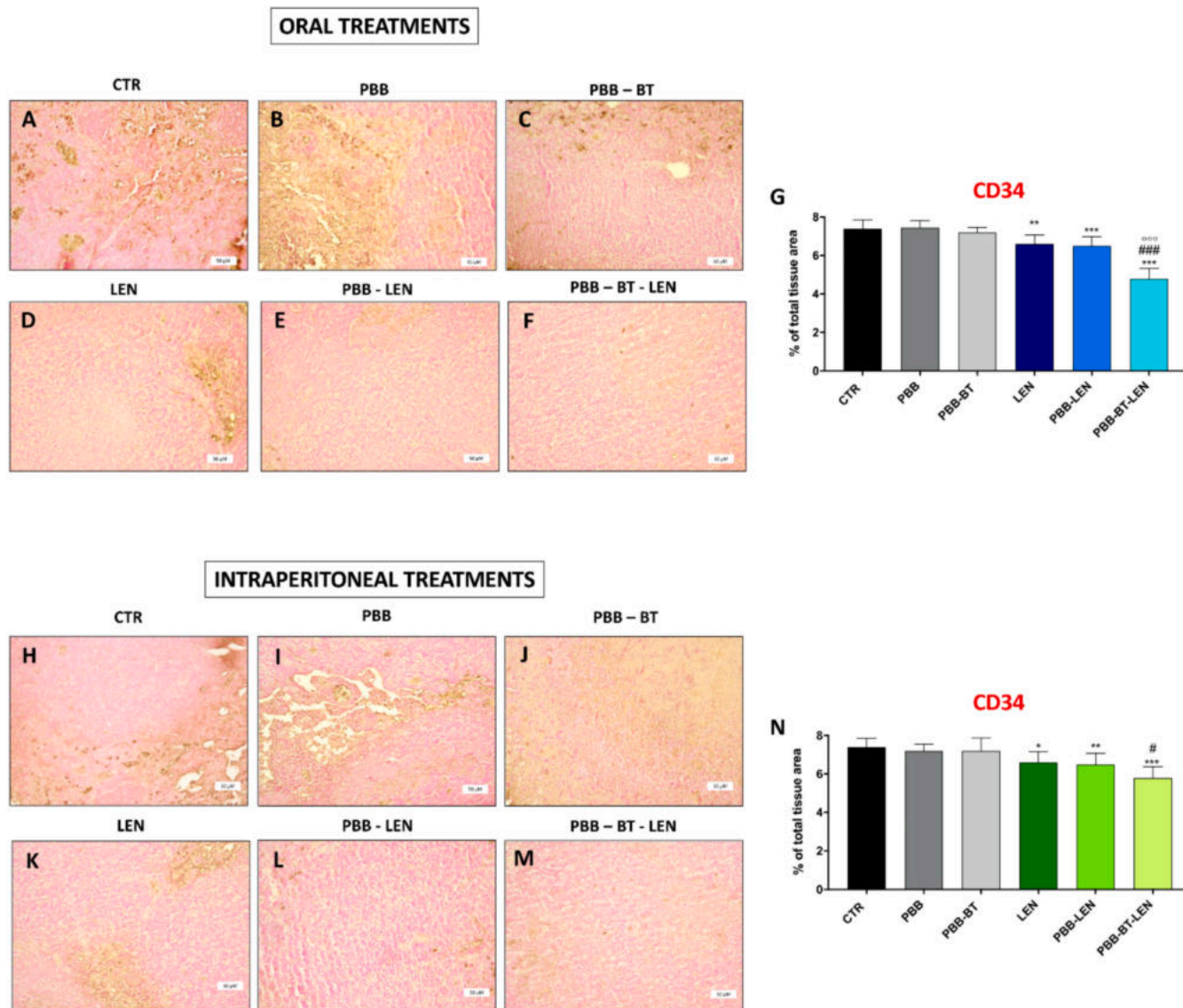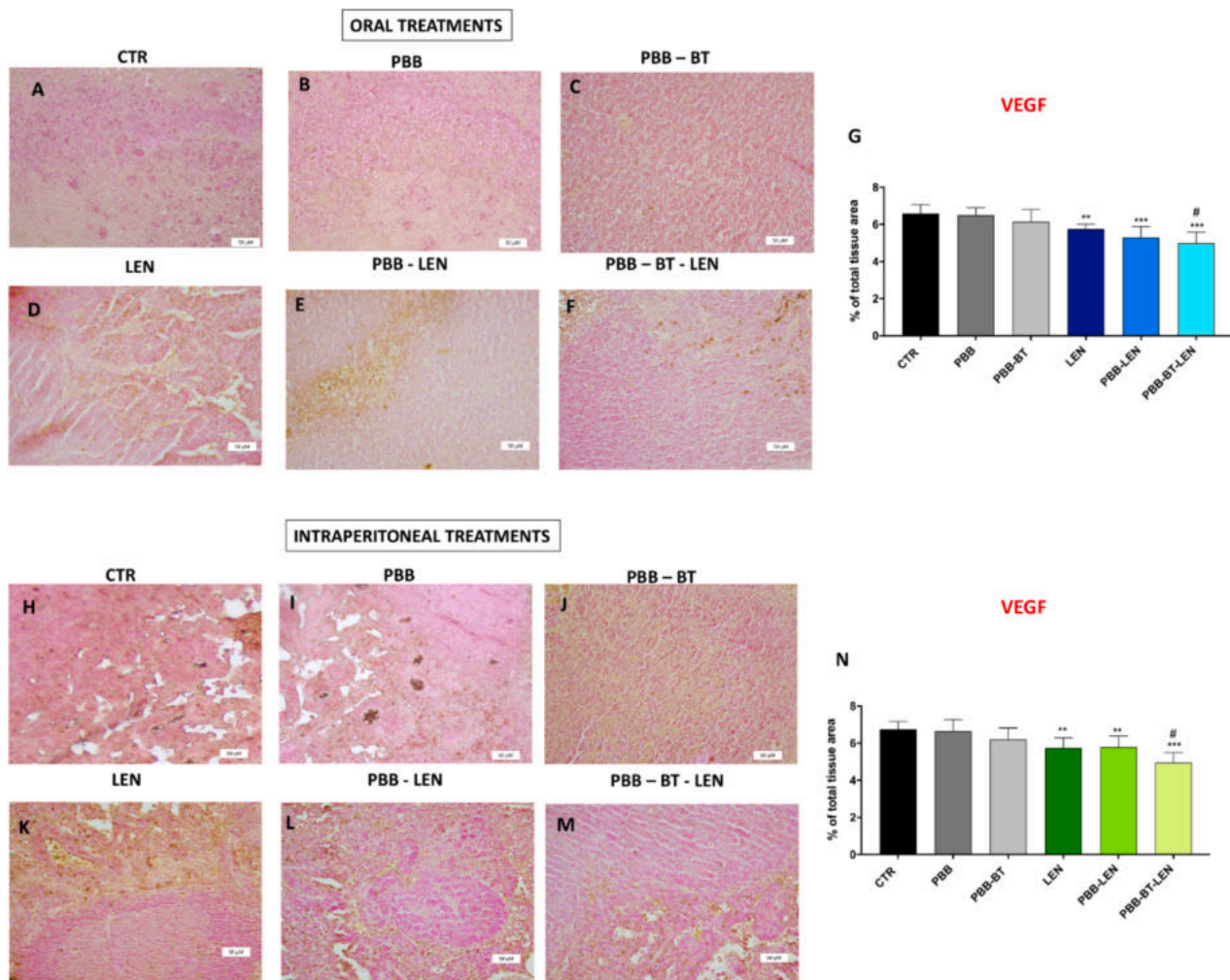
Fig. 6. Immunohistochemical analysis of CD34 following 18 days of treatments. Representative images of angiogenic marker CD34 following oral and intraperitoneal treatments of 18 days. Oral treatments included the following experimental groups: (A) CTR, (B) PBB, (C) PBB-BT, (D) LEN, (E) PBB-LEN, (F) PBB-BT-LEN. Intraperitoneal treatments: (H) CTR group, (I) PBB group, (J) PBB-BT, (K) LEN, (L) PBB-LEN, (M) PBB-BT-LEN. (G) Histological score of oral treatments. (N) Histological score of intraperitoneal treatments. Images are shown at $20 \times$ magnification. Values are means $\pm$ SD. One-way ANOVA test. * $p < 0.05$ vs CTR; ** $p < 0.01$ vs CTR; *** $p < 0.001$ vs CTR; # $p < 0.05$ vs LEN; ### $p < 0.001$ vs LEN; °°° $p < 0.001$ vs PBB-LEN. The scale bar represents 50 µm.

proliferation, the expression of the specific proliferation marker Ki-67 was evaluated by using ELISA kits. Our results demonstrated a considerable expression of Ki-67 marker in CTR mice as well as in animals treated orally for 18 days with PBB and PBB-BT (Fig. 4 panel I). Treatments with LEN, PBB-LEN and PBB-BT-LEN significantly reduced Ki-67 levels, compared to the CTR group (Fig. 4 panel I). Furthermore, oral treatment with PBB-BT-LEN significantly reduced Ki-67 levels compared to free LEN and compared to PBB-LEN (Fig. 4 panel I). Regarding intraperitoneal treatments, the histological analyses highlighted an important tumor mass in mice from CTR group (Fig. 4 panel J, histological score P). Similarly, both PBB and PBB-BT mice did not showed amelioration in morphological tumor features (Fig. 4 panels K-L, histological score P). Differently, a significant reduction of histological damage was observed following 18 days of intraperitoneal treatment with LEN, PBB-LEN and PBB-BT-LEN (Fig. 4 panels M–O, histological score P) compared to CTR group. Moreover, treatment with PBB-BT-LEN significantly reduced histological damage compared to the free LEN and PBB-LEN (histological score P). In addition, the results showed that

intraperitoneal treatment with LEN, PBB-LEN (Fig. 4 panels M–N, histological score P) but especially with PBB-BT-LEN (Fig. 4 panel O, histological score P), significantly reduced the tumor burden compared to CTR group (Fig. 4 panel Q). After intraperitoneal administrations for 18 days, increased expressions of Ki-67 marker in CTR mice, and in PBB and PBB-BT groups were observed (Fig. 4 panel R). LEN, PBB-LEN, and PBB-BT-LEN treatments significantly reduced Ki-67 levels, compared to CTR groups (Fig. 4 panel R). PBB-BT-LEN treatment was more efficacious in reducing Ki-67 levels compared both to LEN and PBB-LEN (Fig. 4 panel R). Taken together, these data demonstrated that PBB-BT-LEN, mainly after oral administration, showed better efficacy in reducing tumor burden, histological damage and Ki-67 levels compared to free LEN and non-targeted nanoparticles PBB-LEN.

3.5.2. Evaluation of apoptotic markers following 18 days of treatment with PBB-LEN and PBB-BT-LEN

Apoptosis plays a key role in cancer progression, thereby targeting apoptotic pathways represents a relevant therapeutic approach in the

Fig. 7. Immunohistochemical staining of VEGF following 18 days of treatments. Representative images of angiogenic marker VEGF following 18-day of oral and intraperitoneal treatments. Experimental groups: (A) CTR, (B) PBB, (C) PBB-BT, (D) LEN, (E) PBB-LEN, (F) PBB-BT-LEN. (G) Histological score. Likewise, intraperitoneal treatments included (H) CTR, (I) PBB, (J) PBB-BT, (K) LEN, (L) PBB-LEN, (M) PBB-BT-LEN. (N) Histological score. Images are shown at 20 × magnification. Values are means ± SD. One-way ANOVA test. ** $p < 0.01$ vs CTR; *** $p < 0.001$ vs CTR; # $p < 0.05$ vs LEN. The scale bar represents 50 μm.

development of anticancer drugs. Thus, we investigated the effect of the treatments on the apoptosis pathway by evaluating pro-apoptotic markers such as Bax, Caspase-3, −8 and −9 and anti-apoptotic marker as Bcl-2 by using Western blot analysis and ELISA assays. The obtained results demonstrated high levels of the anti-apoptotic protein Bcl-2 in the CTR, PBB and PBB-BT groups (Fig. 5 panel A, densitometric analysis 3 A1). Differently, a minimal content of pro-apoptotic proteins such as Bax (Fig. 5 panel B, densitometric analysis 3 B1) and Caspases 3–8-9, were observed in the CTR, PBB and PBB-BT groups (Fig. 5 panels C-E). By contrast, 18-days oral administration of LEN, PBB-LEN and PBB-BT-LEN positively induced apoptotic process favorably increasing pro-apoptotic proteins (Fig. 5 panels B-E) as well as reducing Bcl-2 expression (Fig. 5 panel A, densitometric analysis 3 A1) compared to CTR group. Immunofluorescence analysis showed that 18 days of oral treatments with LEN, PBB-LEN and PBB-BT-LEN significantly increased the number of p53 positive cells compared to CTR, PBB and PBB-BT groups (Fig. 5 panels F-K, score L). In particular, PBB-BT-LEN significantly increased the number of positive cells compared to LEN and PBB-LEN groups (score 3 L). Intraperitoneal administrations of LEN, PBB-LEN and PBB-BT-LEN significantly increased all the pro-apoptotic markers and decreased Bcl-2 compared to the CTR group (Fig. 3 panels N-Q and 3 M, respectively), as demonstrated by Western blot analysis and ELISA assay. Interestingly, it was observed that intraperitoneal treatment with PBB-BT-LEN for 18 days, significantly increased most of the apoptotic

parameters compared to LEN or PBB-LEN treatments (Fig. 3 panels N-Q). At the same way, a better ability to reduce the expression of Bcl-2 anti-apoptotic protein was observed following PBB-BT-LEN treatment when compared to LEN and PBB-LEN administrations (Fig. 5 panel M). Furthermore, a higher number of p53 positive cells was observed in tumor sections of LEN, PBB-LEN, and PBB-BT-LEN treated mice (Fig. 5 panels U-W, score X) when compared with the CTR group (Fig. 5 panels R-T, score X).

3.5.3. Evaluation of angiogenic markers CD34 and VEGF following 18 days of PBB-LEN and PBB-BT LEN treatments

Immunohistochemical analysis of the tumor sections was performed to evaluate the expression of the pro-angiogenic marker CD34 following 18 days of oral treatments. Data revealed a high number of CD34 positive cells in the CTR, PBB and PBB-BT groups (Fig. 6 panels A-C, score G). Otherwise, LEN, PBB-LEN and PBB-BT-LEN were able to reduce the number of CD34 + cells compared to CTR mice (Fig. 6 panels D-F, score G). Especially, it is worthy to underline that PBB-BT-LEN showed more efficacy in reducing the number of CD34 + cells compared to LEN and PBB-LEN (score G). We also evaluated CD34 + cells after 18 days of intraperitoneal treatment with the various formulations. Immunohistochemical analysis showed that intraperitoneal treatment with LEN, PBB-LEN, and PBB-BT-LEN (Fig. 6 panels K-M, score N) considerably reduced the number of CD34 immunopositivity compared to the CTR group
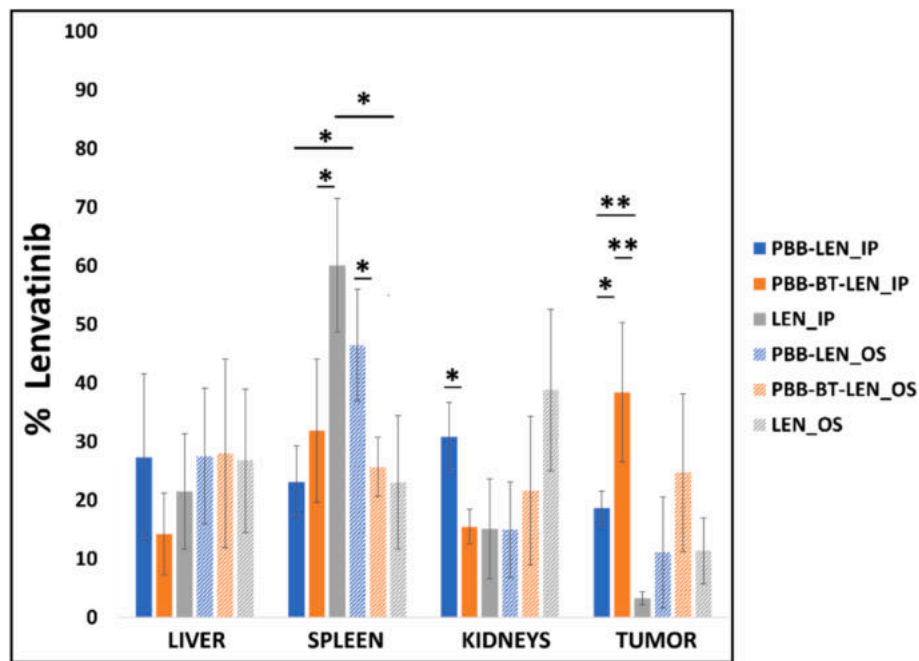
Fig. 8. Lenvatinib biodistribution 18 days after intraperitoneal injections (solid fill) or oral administrations (dashed fill) of PBB-LEN (blue), PBB-BT-LEN (orange) and free lenvatinib (grey) in excised livers, spleens, kidneys, and tumors.

(Fig. 6 panel H, score N). Furthermore, PBB-BT-LEN intraperitoneal treatment had a greater statistical significance in reducing the number of CD34 + cells compared to the free LEN (score N). Whereas, following intraperitoneal administrations no significant reduction was observed between the PBB-LEN and PBB-BT-LEN treatments (score N).

It has been demonstrated that HCC expresses many angiogenic factors, including VEGF and angiogenin, playing an important role in neovessel forming; 60–70 % of human HCCs have shown elevated levels of VEGF expression(Deli et al., 2005). Therefore, immunohistochemistry of VEGF in tumor tissue has been carried out. Mice treated orally for 18 days with LEN, PBB-LEN, and PBB-BT-LEN (Fig. 7 panels D-F, score G) showed a significant decrease in immunopositivity for VEGF compared to CTR mice (Fig. 7 panel A, score G). Furthermore, from the immunohistochemical analyses we reported that oral PBB-BT-LEN had a better efficacy in reducing VEGF immunopositivity than free LEN (score G). In addition, we investigated VEGF expression by immunohistochemical staining also following intraperitoneal administrations. The immunohistochemical analysis of VEGF revealed that mice treated for 18 days with LEN, PBB-LEN and PBB-BT-LEN had decreased number of VEGF+cells (Fig. 7 panels K-M, score N) compared to CTR group (Fig. 7 panel H, score N). Moreover, the intraperitoneal administration of PBB-BT-LEN led to a greater reduction of VEGF+cell compared to the LEN-treated mice (score N).

3.5.4. Biodistribution

At the end of the experiment, excised organs were analyzed to assess how the delivery of lenvatinib influenced its distribution into the tissues. As shown in Fig. 8, free drug administered intraperitoneally exhibited substantial accumulation in the spleen, a phenomenon significantly reduced when the drug was delivered through nanoparticles or administered orally. On the other hand, no significant differences were observed in the hepatic accumulation of lenvatinib for all treated groups. Interestingly, notable findings emerged from the study of the biodistribution in tumors. Specifically, intraperitoneal administration showed that the free drug accumulated in the tumor mass is significantly lower than lenvatinib delivered by nanoparticles. Furthermore, the accumulation observed after the administration of nanoparticles bearing biotin as a targeting agent (PBB-BT-LEN) is statistically significant even

when compared to non-targeted nanoparticles. This result suggests that biotin conjugation has ensured more effective and selective delivery of lenvatinib to the hepatocellular carcinoma xenograft, thus confirming the success the system with active targeting properties.

4. Conclusions

In this study, nanoparticles loaded with lenvatinib have been prepared using a ATRP synthesized amphiphilic polyaminoacidic-based graft copolymer (PHEA-g-BIB-pButMA-g-PEG-Bt). This nanosystem was designed for biotin-mediated active targeting towards cancer cells that overexpress the biotin receptor, aiming to achieve effective loading and localized release of substantial amounts of the hydrophobic anticancer drug lenvatinib. Lenvatinib was incorporated into the hydrophobic core of the nanoparticles (PBB-BT-LEN) through mortar-pestle grinding giving rise to nanosystems exhibiting a diameter suitable for a parenteral and oral administration, satisfactory drug loading and extended drug release capabilities. The in vivo efficacy was evaluated after 3, 7 and 18 days of treatment, both orally and intraperitoneally, by assessing tumour burden, histological scores, apoptotic and proangiogenic markers. After 3 days of treatment, no statistically significant differences were observed in the parameters analyzed, while after 7 days of treatment, it was observed a greater pharmacological efficacy in the groups treated with PBB-LEN, PBB-BT-LEN or free lenvatinib compared to the control animal group, but no significant differences were found between the of free lenvatinib and the drug delivery systems. On the other hand, the data obtained after 18 days of treatments showed statistically significant differences between free lenvatinib and the respective PBB-LEN and PBB-BT-LEN systems, showing a greater reduction in tumour volume and histological damage, as well as an increase in all pro-apoptotic markers, in association with a reduction of the anti-apoptotic protein Bcl-2, the marker Ki-67 and the proangiogenic markers CD34 and VEGF. Interestingly, the biotinylated PBB-BT-LEN system resulted significantly more effective than the nontargeted PBB-LEN system for all parameters evaluated, due to increased accumulation of targeted systems in the tumor mass, as demonstrated by biodistribution studies. Therefore, these results indicate that the proposed nanoparticles can be considered promising

candidates for targeted therapy of hepatocarcinoma.

Author contributions

P.Varvarà: Investigation, data curation, formal analysis, writing original draft; S.E.Drago: Investigation, data curation, formal analysis, writing original draft; E. Esposito: Biological experimental design, data and statistical analysis, writing-review and editing; M. Campolo: performed in vivo experiment, writing original draft; N.Mauro: Methodology, supervision, writing-review & editing; G. Calabrese: performed in vitro experiment, writing original draft; S. Conoci: funding acquisition, project administration, and writing—review and editing; D. Morganti: performed Raman experiment; B. Fazio: performed Raman experiment; G.Giammona: Conceptualization, supervision, funding acquisition; G. Pitarresi: Funding acquisition, supervision, writing-review and editing. All authors have read and agreed to the published version of the manuscript.

Funding

CRediT authorship contribution statement

Paola Varvarà: Writing – original draft, Investigation, Formal analysis, Data curation. **Salvatore Emanuele Drago:** Writing – original draft, Investigation, Formal analysis, Data curation. **Emanuela Esposito:** Writing – review & editing, Formal analysis, Data curation. **Michela Campolo:** Writing – original draft, Investigation. **Nicolò Mauro:** Writing – review & editing, Supervision, Methodology. **Giovanna Calabrese:** Writing – original draft, Investigation. **Sabrina Conoci:** Writing – review & editing, Project administration, Funding acquisition. **Dario Morganti:** Investigation. **Barbara Fazio:** Investigation. **Gaetano Giammona:** Supervision, Funding acquisition, Conceptualization. **Giovanna Pitarresi:** Writing – original draft, Investigation.

Declaration of competing interest

The authors declare that they have no known competing financial interests or personal relationships that could have appeared to influence the work reported in this paper.

Data availability

No data was used for the research described in the article.

Acknowledgments

Appendix A. Supplementary data

Supplementary data to this article can be found online at https://doi.org/10.1016/j.ijpharm.2024.124537.

References

Al-Salama, Z.T., Syed, Y.Y., Scott, L.J., 2019. Lenvatinib: A Review in Hepatocellular Carcinoma. Drugs 79, 665–674. https://doi.org/10.1007/S40265-019-01116-X.

Anwanwan, D., Singh, S.K., Singh, S., Saikam, V., Singh, R., 2020. Challenges in liver cancer and possible treatment approaches. Biochim. Biophys. Acta 1873. https://doi.org/10.1016/j.bbcan.2019.188314.

Ardizzone, A., Filippone, A., Mannino, D., Scuderi, S.A., Casili, G., Lanza, M., Cucinotta, L., Campolo, M., Esposito, E., 2022. Ulva pertusa, a Marine Green Alga, Attenuates DNBS-Induced Colitis Damage via NF-κB/Nrf2/SIRT1 Signaling Pathways. J. Clin. Med. 11, 4301. https://doi.org/10.3390/JCM11154301/S1.

Ardizzone, A., Mannino, D., Capra, A.P., Repici, A., Filippone, A., Esposito, E., Campolo, M., 2023. New Insights into the Mechanism of Ulva pertusa on Colitis in Mice: Modulation of the Pain and Immune System. Mar. Drugs 21, 298. https://doi.org/10.3390/MD21050298/S1.

Borodko, Y., Habas, S.E., Koebel, M., Yang, P., Frei, H., Somorjai, G.A., 2006. Probing the interaction of poly(vinylpyrrolidone) with platinum nanocrystals by UV - Raman and FTIR. J. Phys. Chem. B 110, 23052–23059. https://doi.org/10.1021/JP063338.

Böttger, R., Pauli, G., Chao, P.H., Fayez, A.L., Hohenwarter, N., Li, S.D., 2020. Lipid-based nanoparticle technologies for liver targeting. Adv. Drug Deliv. Rev. 154–155, 79–101. https://doi.org/10.1016/J.ADDR.2020.06.017.

Bruix, J., da Fonseca, L.G., Reig, M., 2019. Insights into the success and failure of systemic therapy for hepatocellular carcinoma. Nat. Rev. Gastroenterol. Hepatol. 16, 617–630. https://doi.org/10.1038/S41575-019-0179-X.

Campolo, M., Casili, G., Lanza, M., Filippone, A., Cordaro, M., Ardizzone, A., Scuderi, S. A., Cuzzocrea, S., Esposito, E., Paterniti, I., 2021. The inhibition of mammalian target of rapamycin (mTOR) in improving inflammatory response after traumatic brain injury. J. Cell Mol. Med. 25, 7855–7866. https://doi.org/10.1111/JCMM.16702.

Capozzi, M., De Divitiis, C., Ottaiano, A., Von Arx, C., Scala, S., Tatangelo, F., Delrio, P., Tafuto, S., 2019. Lenvatinib, a molecule with versatile application: from preclinical evidence to future development in anti-cancer treatment. Cancer Manag. Res. 11, 3847. https://doi.org/10.2147/CMAR.S188316.

Cervello, M., Pitarresi, G., Volpe, A.B., Porsio, B., Balasus, D., Emma, M.R., Azzolina, A., Puleio, R., Loria, G.R., Puleo, S., Giammona, G., 2017. Nanoparticles of a polyaspartamide-based brush copolymer for modified release of sorafenib: In vitro and in vivo evaluation. J. Control. Release 266, 47–56. https://doi.org/10.1016/J.JCONREL.2017.09.014.

Chen, P., Kuang, W., Zheng, Z., Yang, S., Liu, Y., Su, L., Zhao, K., Liang, G., 2019. Carboxylesterase-Cleavable Biotinylated Nanoparticle for Tumor-Dual Targeted Imaging. Theranostics 9, 7359–7369. https://doi.org/10.7150/THNO.37625.

Daher, S., Massarwa, M., Benson, A.A., Khoury, T., 2018. Current and Future Treatment of Hepatocellular Carcinoma: An Updated Comprehensive Review. J. Clin. Transl. Hepatol. 6, 69. https://doi.org/10.14218/JCTH.2017.00031.

Deli, G., Jin, C.H., Mu, R., Yang, S., Liang, Y., Chen, D., Makuuchi, M., 2005. Immunohistochemical assessment of angiogenesis in hepatocellular carcinoma and surrounding cirrhotic liver tissues. World J. Gastroenterol. 11, 960–963. https://doi.org/10.3748/wjg.v11.i7.960.

Filippone, A., Casili, G., Scuderi, S.A., Mannino, D., Lanza, M., Campolo, M., Paterniti, I., Capra, A.P., Colarossi, C., Bonasera, A., Lombardo, S.P., Cuzzocrea, S., Esposito, E., 2022. Sodium Propionate Contributes to Tumor Cell Growth Inhibition through PPAR-γ Signaling. Cancers 2023, Vol. 15, Page 217 15, 217. https://doi.org/10.3390/CANCERS15010217.

Finn, R., 2013. Emerging targeted strategies in advanced hepatocellular carcinoma. Semin. Liver Dis. 33 https://doi.org/10.1055/S-0033-1333632.

Fu, C., Yang, R.M., Wang, L., Li, N.N., Qi, M., Xu, X.D., Wei, X.H., Jiang, X.Q., Zhang, L. M., 2017. Surface functionalization of superparamagnetic nanoparticles by an acid-liable polysaccharide-based prodrug for combinatorial monitoring and chemotherapy of hepatocellular carcinoma. RSC Adv. 7, 41919–41928. https://doi.org/10.1039/c7ra05042a.

Giammona, G., Carlisi, B., Palazzo, S., 1987. Reaction of α, β-poly(N-hydroxyethyl)-DL-aspartamide with derivatives of carboxylic acids. J. Polym. Sci. A Polym. Chem. 25, 2813–2818. https://doi.org/10.1002/pola.1987.080251016.

Giammona, G., Drago, S.E., Calabrese, G., Varvarà, P., Rizzo, M.G., Mauro, N., Nicotra, G., Conoci, S., Pitarresi, G., 2022. Galactosylated Polymer/Gold Nanorods Nanocomposites for Sustained and Pulsed Chemo-Photothermal Treatments of Hepatocarcinoma. Pharmaceutics 14, 2503. https://doi.org/10.3390/pharmaceutics14112503.

Ho, S.Y., Liu, P.H., Hsu, C.Y., Huang, Y.H., Lei, H.J., Liao, J.I., Su, C.W., Hou, M.C., Huo, T.I., 2023. Surgical resection versus transarterial chemoembolization for patients with hepatocellular carcinoma beyond Milan criteria: prognostic role of tumor burden score. Scientific Reports 2023 13:1 13, 1–9. https://doi.org/10.1038/s41598-023-41068-7.

Hu, Y.W., Du, Y.Z., Liu, N., Liu, X., Meng, T.T., Cheng, B.L., He, J.B., You, J., Yuan, H., Hu, F.Q., 2015. Selective redox-responsive drug release in tumor cells mediated by chitosan based glycolipid-like nanocarrier. J. Control. Release 206, 91–100. https://doi.org/10.1016/J.JCONREL.2015.03.018.

Hu, X., Zhu, H., He, X., Chen, J., Xiong, L., Shen, Y., Li, J., Xu, Y., Chen, W., Liu, X., Cao, D., Xu, X., 2023. The application of nanoparticles in immunotherapy for hepatocellular carcinoma. J. Control. Release 355, 85–108. https://doi.org/10.1016/J.JCONREL.2023.01.051.

Jemal, A., Bray, F., Center, M.M., Ferlay, J., Ward, E., Forman, D., 2011. Global cancer statistics. CA Cancer J. Clin. 61, 69–90. https://doi.org/10.3322/CAAC.20107.

Landesman-Milo, D., Peer, D., 2016. Transforming Nanomedicines from Lab Scale Production to Novel Clinical Modality. Bioconjug. Chem. 27, 855–862. https://doi.org/10.1021/ACS.BIOCONJCHEM.5B00607.

Lee, Y.H., Hsia, C.Y., Hsu, C.Y., Huang, Y.H., Lin, H.C., Huo, T.I., 2013. Total tumor volume is a better marker of tumor burden in hepatocellular carcinoma defined by the Milan criteria. World J. Surg. 37, 1348–1355. https://doi.org/10.1007/S00268-013-1978-9.

Liu, Y., Li, J., Liu, F., Zhang, L., Feng, L., Yu, D., Zhang, N., 2015. Theranostic polymeric micelles for the diagnosis and treatment of hepatocellular carcinoma. J. Biomed. Nanotechnol. 11, 613–622. https://doi.org/10.1166/jbn.2015.1945.

Llovet, J.M., Kelley, R.K., Villanueva, A., Singal, A.G., Pikarsky, E., Roayaie, S., Lencioni, R., Koike, K., Zucman-Rossi, J., Finn, R.S., 2021. Hepatocellular carcinoma. Nature Reviews Disease Primers 2021 7:1 7, 1–28. https://doi.org/10.1038/s41572-020-00240-3.

Llovet, J.M., Pinyol, R., Kelley, R.K., El-Khoueiry, A., Reeves, H.L., Wang, X.W., Gores, G. J., Villanueva, A., 2022. Molecular pathogenesis and systemic therapies for hepatocellular carcinoma. Nat Cancer 3, 386–401. https://doi.org/10.1038/S43018-022-00357-2.

Luo, X., Ao, S., Li, C., Fang, L., Chen, L., Liu, H., Li, J., Zhou, Y., Yin, X., Wu, C., Xi, M., Zhu, K., 2023. Enhanced delivery of lenvatinib by hyaluronic acid-polyglycerol-stearate self-assembled micelles to inhibit hepatocellular carcinoma in vitro. J Drug Deliv Sci Technol 86, 104631. https://doi.org/10.1016/J.JDDST.2023.104631.

Mauro, N., Utzeri, M.A., Cillari, R., Scialabba, C., Giammona, G., Cavallaro, G., 2022. Cholesterol-Inulin Conjugates for Efficient SN38 Nuclear Delivery: Nanomedicines for Precision Cancer Therapy. Cancers (basel) 14, 4857. https://doi.org/10.3390/cancers14194857.

Metkar, S.P., Fernandes, G., Navti, P.D., Nikam, A.N., Kudarha, R., Dhas, N., Seetharam, R.N., Santhosh, K.V., Rao, B.S.S., Mutalik, S., 2023. Nanoparticle drug delivery systems in hepatocellular carcinoma: A focus on targeting strategies and therapeutic applications. OpenNano 12, 100159. https://doi.org/10.1016/J.ONANO.2023.100159.

Ogasawara, S., Mihara, Y., Kondo, R., Kusano, H., Akiba, J., Yano, H., 2019. Antiproliferative Effect of Lenvatinib on Human Liver Cancer Cell Lines In Vitro and In Vivo. Anticancer Res 39, 5973–5982. https://doi.org/10.21873/ANTICANRES.13802.

Scarabel, L., Perrone, F., Garziera, M., Farra, R., Grassi, M., Musiani, F., Russo Spena, C., Salis, B., De Stefano, L., Toffoli, G., Rizzolio, F., Tonon, F., Abrami, M., Chiarappa, G., Pozzato, G., Forte, G., Grassi, G., Dapas, B., 2017. Strategies to optimize siRNA delivery to hepatocellular carcinoma cells. Expert Opin. Drug Deliv. 14, 797–810. https://doi.org/10.1080/17425247.2017.1292247.

Scuderi, S.A., Casili, G., Ardizzone, A., Forte, S., Colarossi, L., Sava, S., Paterniti, I., Esposito, E., Cuzzocrea, S., Campolo, M., 2021. KYP-2047, an inhibitor of prolyl-oligopeptidase, reduces glioblastoma proliferation through angiogenesis and apoptosis modulation. Cancers (basel) 13, 3444. https://doi.org/10.3390/CANCERS13143444/S1.

Singh, A., Mishra, S., Sharma, S., Ojha, S., Yagnik, S., Pandey, S., 2023. Ligand-mediated Targeted Drug Delivery Approaches against Hepatocellular Carcinoma. Curr. Cancer Drug Targets 23, 879–888. https://doi.org/10.2174/1568009623666230503094346.

Wang, H., Bo, W., Feng, X., Zhang, J., Li, G., Chen, Y., 2024. Strategies and Recent Advances on Improving Efficient Antitumor of Lenvatinib Based on Nanoparticle Delivery System. Int. J. Nanomed. 19, 5581–5603. https://doi.org/10.2147/IJN.S460844.

Wang, Y.Q., Huang, C., Ye, P.J., Long, J.R., Xu, C.H., Liu, Y., Ling, X.L., Lv, S.Y., He, D.X., Wei, H., Yu, C.Y., 2022. Prolonged blood circulation outperforms active targeting for nanocarriers-mediated enhanced hepatocellular carcinoma therapy in vivo. J. Control. Release 347, 400–413. https://doi.org/10.1016/J.JCONREL.2022.05.024.

Yu, Z., Huang, L., Guo, J., 2024. Anti-stromal nanotherapeutics for hepatocellular carcinoma. J. Control. Release 367, 500–514. https://doi.org/10.1016/J.JCONREL.2024.01.050.

Zhao, Y., Zhang, Y.N., Wang, K.T., Chen, L., 2020. Lenvatinib for hepatocellular carcinoma: From preclinical mechanisms to anti-cancer therapy. Biochimica et Biophysica Acta (BBA) - Reviews on. Cancer 1874, 188391. https://doi.org/10.1016/J.BBCAN.2020.188391.